Landslides (2020) 17:2631–2641
DOI 10.1007/s10346-020-01506-3
Received: 30 December 2019
Accepted: 31 July 2020
Published online: 11 August 2020

Francis K. Rengers · Luke A. McGuire · Nina S. Oakley · Jason W. Kean · Dennis M. Staley · Hui Tang

Landslides after wildfire: initiation, magnitude, and mobility

Abstract In the semiarid Southwestern USA, wildfires are commonly followed by runoff-generated debris flows because wildfires remove vegetation and ground cover, which reduces soil infiltration capacity and increases soil erodibility. At a study site in Southern California, we initially observed runoff-generated debris flows in the first year following fire. However, at the same site three years after the fire, the mass-wasting response to a long-duration rainstorm with high rainfall intensity peaks was shallow landsliding rather than runoff-generated debris flows. Moreover, the same storm caused landslides on unburned hillslopes as well as on slopes burned 5 years prior to the storm and areas burned by successive wildfires, 10 years and 3 years before the rainstorm. The landslide density was the highest on the hillslopes that had burned 3 years beforehand, and the hillslopes burned 5 years prior to the storm had low landslide densities, similar to unburned areas. We also found that reburning (i.e., two wildfires within the past 10 years) had little influence on landslide density. Our results indicate that landscape susceptibility to shallow landslides might return to that of unburned conditions after as little as 5 years of vegetation recovery. Moreover, most of the landslide activity was on steep, equatorial-facing slopes that receive higher solar radiation and had slower rates of vegetation regrowth, which further implicates vegetation as a controlling factor on post-fire landslide susceptibility. Finally, the total volume of sediment mobilized by the year 3 landslides was much smaller than the year 1 runoff-generated debris flows, and the landslides were orders of magnitude less mobile than the runoff-generated debris flows.

Keywords Landslide · Wildfire · Geomorphology

Introduction

Wildfire disturbs normal hydrologic and soil conditions. Burned forest soils often repel water, causing fire-induced reductions in infiltration (DeBano et al. 1979; DeBano 2000; Ebel and Moody 2016; McGuire et al. 2018), leading to an increased likelihood of flooding and runoff-generated debris flows (Wells 1987). This is commonly described as the "fire–flood cycle" (Kotok and Kraebel 1935). Post-fire debris flows, in particular, can be lethal hazards, resulting in high numbers of fatalities (Dowling and Santi 2014; Eaton 1935; Kean et al. 2019a).

Post-fire landslides have also been observed. Scott (1971) documented several landslides in areas that had burned the prior year, but the storm that triggered the landslides also triggered landslides in many unburned areas (Campbell 1975). Several additional authors have observed landslides in areas that burned 5 or more years beforehand (Benda and Dunne 1997; May and Gresswell 2003; Meyer et al. 2001; Rice and Foggin 1971). These landslides can subsequently transition into debris flows (De Graff 2018; Jackson and Roering 2009; Woodsmith et al. 2004, 2007). The increase in landslide susceptibility after wildfire has been attributed to increases in soil moisture that persists for several years after wildfire as a result of decreased evapotranspiration (Helvey 1980). In addition, researchers have found that roots can lose strength following fire, thereby reducing the apparent cohesion provided by roots and leaving hillslopes more prone to failure (De Graff 2018; Gehring et al. 2019; Jackson and Roering 2009; Lanini et al. 2009; Regelbrugge and Conard 1993). Modeling studies have shown that post-fire landslides are an important contributor of sediment to low-order channels (Martin 2007).

Understanding the conditions leading to landsliding after wildfire is important due to the hazard that landslides pose to life and infrastructure (Froude and Petley 2018; Petley 2012). Landslides also play an important geomorphic role in the evolution of mountainous landscapes (Densmore et al. 1997; Lavé and Burbank 2004; Schmidt and Montgomery 1995). Landslides can be the primary mechanism contributing coarse sediment to channels, and this material is crucial for facilitating bedrock channel erosion (Attal et al. 2015; Egholm et al. 2013). Moreover, sediment mobilized by landsliding influences the long-term morphology of downstream channel reaches (Korup 2004; Lévy et al. 2012; Ouimet et al. 2007). Consequently, research into the timing and mobility of post-fire landsliding is becoming increasingly important as wildfires increase in size and frequency (Gillett et al. 2004; Hu et al. 2010; Kasischke and Turetsky 2006; Miller et al. 2009; Pausas and Fernández-Muñoz 2012; Westerling et al. 2006).

In this study, we document a set of shallow landslides in the San Gabriel Mountains, California, USA, that were initiated by a rainstorm in January 2019. This rainstorm led to landslides in areas that were (i) unburned, (ii) burned 3 years beforehand, (iii) burned 5 years beforehand, and (iv) burned by successive wildfires 10 years and 3 years prior. Prior research in Southern California chaparral-dominated ecosystems has found that the number of rainfall-induced shallow landslides was five times greater on more sparsely vegetated south- and west-facing slopes (Corbett and Rice 1966). The dataset presented here provides an opportunity to explore the influence of slope aspect on landsliding after wildfire. These landslide observations also provide an opportunity to compare the magnitude, mobility, and initiation style of post-fire landslides across slopes in various stages of vegetation/hydrologic recovery. Specifically, we use the dataset to explore the following research questions: (1) whether landslide density is influenced by burn severity, (2) how the density and runout of landslides vary with years of post-fire recovery, and (3) whether landslides cluster in areas based on geomorphic metrics (e.g., slope, aspect).

Study site and previous work

Our study area is in the San Gabriel Mountains in Southern California, USA, and encompasses an area of approximately 70 km^2 (Fig. 1). The San Gabriel Mountains are situated in a

Mediterranean climate and receive most precipitation during the winter. The soils in the region are typically composed of gravelly sandy loams (Web Soil Survey 2020).

The dominant vegetation type in the area is chaparral, which is a drought-resistant ecosystem composed of sclerophyllous woody shrubs (Halsey 2005). This vegetation has a relatively shallow rooting depth, with 90% of the root mass occurring within 40 cm of the surface; however, roots can penetrate and extend into underlying bedrock (Kummerow et al. 1977). Chaparral plants are relatively resilient to wildfires. Some species such as Toyon (*Heteromeles arbutifolia*) and holly-leafed cherry (*Prunus ilicifolia*) are known as obligate resprouters and can resprout directly from burned roots (Halsey 2005). Facultative seeders, such as chamise (*Adenostoma fasciculatum*) and whitebark ceanothus (*Ceanothus leucodermis*), can resprout from burned roots as well; however, seeds produced by facultative seeders can also survive fire, and germination is stimulated by heat (Halsey 2005). Finally, some chaparral plants such as cupleaf ceanothus (*Ceanothus greggii*) and bigberry manzanita (*Arctostaphylos glauca*) are obligate seeders (Halsey 2005). During a wildfire, obligate seeders will die, but their seeds respond to fire-related triggers such as heat and smoke, encouraging new plants to grow after the fire. Consequently, the unique fire adaptations of chaparral plants to wildfire often allow the plants to regrow quickly after a fire.

The study site includes areas burned by the 2009 Morris fire (started on 25 August 2009 with a total burn area of 8.8 km^2), the 2014 Colby fire (started on 17 January 2014 with a total burn area of 11.5 km^2), and the 2016 San Gabriel Complex (SGC) fire (started 20 June 2016 with a total burned area of 21 km^2). The SGC fire is a general name for two separate fires that burned together, the Fish and Reservoir fires. In addition, the SGC fire also reburned the area previously burned by the Morris fire. The areas burned by the SGC and Colby fires are primarily underlain by similar geology: the San Gabriel Reservoir tonalite and layered gneiss units (Morton and Miller 2003). The geology that underlies the Morris fire and the portion of the SGC that reburned the Morris is dominated by the Pelona Schist and a gneissic granodiorite (Morton and Miller 2003). Above-ground vegetation was entirely consumed in portions of the burn areas with moderate and high severity. However, in the years following the fires, the burned areas experienced vegetation regrowth. No data are available to estimate the depth of heat penetration during the burn, but prior studies in Southern California show high temperatures (> 110 °C) up to 10 cm below the surface (Rengers et al. 2017), and high heat is known to kill fine roots near the soil surface that promote soil stability (Nyman et al. 2013).

The 2016 SGC fire was monitored for overland flow, runoff-generated debris flows, and landslide activity (Kean et al. 2019b). In one watershed within the SGC fire perimeter (Las Lomas, Fig. 1), we observed 11 debris flows during seven precipitation events in the first wet season after the wildfire (Tang et al. 2019). Observations and model simulations from the site showed that the runoff-generated debris flows were initiated via channel-bed mass failure and grain-by-grain progressive entrainment of sediment. Moreover, 15-min rainfall intensities that exceeded the regional threshold for post-fire, runoff-generated debris flows (approximately 19 mm/h) generated debris flows via runoff for all storms in the first wet season (Tang et al. 2019). During the second wet season after the wildfire, no runoff-generated debris flows were observed. Widespread shallow landsliding was observed in the third year after the wildfire.

Methods

Mapping landslides

We mapped landslides that occurred following a rainstorm on 16–17 January 2019 within our 70-km^2 study area using orthophotos (30-cm pixel size) and airborne lidar data (50-cm pixel size). The orthophotos were obtained from DigitalGlobe (https://www.digitalglobe.com/) imagery before any widespread landsliding (26 September 2018) and after landslide initiation (11 February 2019). Landslides were identified by their spectral contrast with the background vegetation and were only mapped if they appeared in imagery captured on 11 February and not in the 26 September imagery. Airborne lidar was collected during 11–24 August 2017 prior to the landslides, and a lidar-derived digital elevation model was used to visually aid with landslide mapping by helping to interpret the locations of landslides and to distinguish between unvegetated areas such as dirt roads and landslides. We used the airborne lidar data to look for trends in the landslide scarp locations to quantify any large-scale landscape controls on the landslide location. In particular, we calculated the hillslope aspect for each landslide main scarp (sensu Varnes 1978) as well as the pre-failure slope angle at the scarp location.

For each landslide, we mapped the top of the main scarp, the slide toe, and a polygon encompassing the landslide failure source area. We used the mapped locations to estimate the landslide density in different parts of the study area (unburned and burned during different wildfires). In addition, the landslide polygons were used to explore the role of burn severity on landslide initiation. Landslide volumes were estimated for the Las Lomas watershed (0.12 km^2, Fig. 1) using the landslide polygons in order to directly compare the landslide volumes with estimates of the runoff-generated debris flow volumes in the same watershed during the first year after fire (Staley et al. 2018). The landslide volumes were estimated by multiplying the size of the mapped source area of each landslide by the average landslide depth measured in the field.

Landslide mobility is typically characterized using the Fahrböschung or angle of reach, which is the angle of a line connecting the landslide main scarp to the most distal portion of the landslide toe (Dai and Lee 2002). The tangent of the angle of reach tends to be inversely related to landslide volume (Corominas 1996), and the travel distance of landslides increases in areas that are unobstructed, are steep, and have a rapid failure mechanism (e.g., debris avalanches tend to move farther than earth flows) (Corominas 1996). Mobility also varies as a function of debris properties and hydrologic properties (Rickenmann 2005). The mapping was used to calculate the tangent of the angle of reach for each landslide using H/L measurements (Corominas 1996), where H is the change in vertical height between the landslide scarp and the landslide toe, and L is the horizontal runout length. To determine L, we mapped the curvilinear path of the landslide centerline and calculated the horizontal distance of that line, similar to the approach described by Coe et al. (2018). This metric provides a comparison of the mobility of the landslides in this burned setting compared with landslides in other settings (Corominas 1996; Legros 2002; Rickenmann 2005) or even other

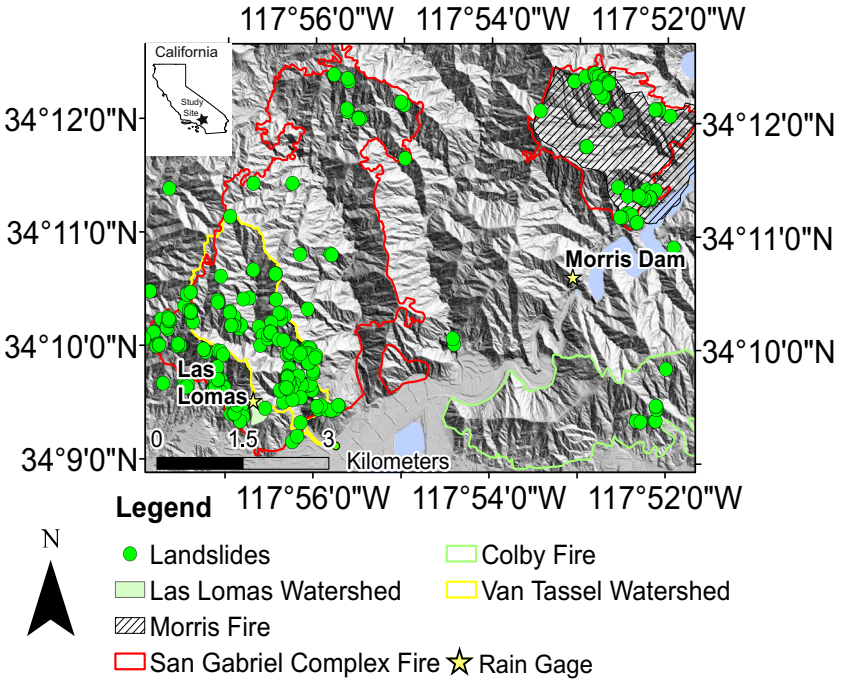

Fig. 1 Map of landslide locations, wildfire outlines, and the study watershed. Inset: location of study site within the state of California, USA

types of mass failure such as rock avalanches (Coe et al. 2018). The *H*/*L* values were used to examine landslide mobility based on the time since burning and reburning, and burned/unburned areas. We evaluated mobility by using a Kruskal–Wallis test to probe for statistical differences between the four groups of landslides (burned in 2016, burned in both 2009 and 2016, burned in 2014, and unburned).

In order to contrast the effectiveness of the landslide transport in year 3 to debris flow transport in year 1, we compared the *H*/*L* of the landslides with runoff-generated debris flows in the Van Tassel watershed (4.2 km^2) in the SGC fire. This watershed was chosen because it is not blocked by a debris basin, and therefore, the sediment deposition from debris flows reflects an unobstructed runout distance. To generate the *H*/*L* for the runoff-generated debris flows in year 1, we used 357 channel heads as the starting point for our estimation of *H* and *L*, based on prior studies revealing channel heads as an initiation point for debris flows (Hyde et al. 2014). We used the canyon outlet of the Van Tassel watershed as the debris flow end point for our calculation of *H* and *L* based on deposition we saw in a horse corral at the canyon outlet.

Field verification of landslides

Field investigation of the landslides was conducted to confirm the presence of slope failures identified in satellite imagery. Field measurements of landslide length, width, and depth were taken at 31 main scarps. In addition, the rooting depth was measured at 19 landslides in the field.

Wildfire influence on landslides

We explored the influence of wildfire and burn severity on each of the mapped landslide. Using the landslide polygons, we determined the percent of each landslide polygon that was burned or unburned. Similarly, we calculated the proportion of each landslide polygon that occupied an area burned at high/moderate severity versus low severity/unburned. Burn severity is a key parameter used to indicate the likelihood of debris flows (Cannon et al. 2010; Staley et al. 2013; Staley et al. 2017), and therefore, we expect that it also could influence landsliding. Burn severity is a scaled categorical index based on both remotely sensed data, such as the differenced normalized burn ratio (dNBR) (Cocke et al. 2005) and field observations (Hudak et al. 2004; Key and Benson 2004). The dNBR is the change in the pre- versus post-fire normalized burn ratio (NBR), which is defined as:

$$\mathrm{NBR} = \frac{\mathrm{NIR}-\mathrm{SWIR}}{\mathrm{NIR}+\mathrm{SWIR}}$$

where NIR is the near-infrared band of an image, and SWIR is the shortwave-infrared band of an image. Qualitative indices based on surface conditions are used to field check the dNBR in order to define the burn severity. For example, areas with low burn severity have organic layers that are not fully consumed, soil aggregate stability, unburned roots, and portions of green canopy in the overlying vegetation (Parsons et al. 2010). By contrast, in areas burned at moderate severity more than 80%, the surface litter and ground fuels are consumed, fine roots (< 0.25 cm) are often scorched, and the canopy shows signs of scorching (Parsons et al. 2010). A high-severity fire fully consumes litter and the duff layer on the soil surface as well as nearly all the ground fuel, the tree roots show signs of char (> 80 mm), and the soil aggregate structure is disturbed (Parsons et al. 2010).

Rainfall

The presence of new landslides in the post-event imagery showed that a rainstorm starting on 16 January 2019 produced the landslides described here. Rainfall began over the study area on 16 January 2019 (local time) with peak rainfall occurring on 17 January 2019. This was the only major rainstorm to impact the area between the 26 September 2018 imagery collection date and 11 February 2019 imagery, and an eyewitness account further confirmed that landslide scars appeared following this storm. We used rainfall data from three tipping bucket rain gages to calculate the cumulative rainfall during the storm as well as the 15-min rainfall intensity.

Results

Observed landslides

We identified 286 landslides in the study area (Fig. 1). Most of the mapped landslides were located in the San Gabriel Reservoir tonalite or layered gneiss (Morton and Miller 2003). Generally, the slides had a well-defined scarp that showed mass detachment and translational downhill movement. The slides initiated within 4.8 m from hillslope ridgetops, on average. However, the masses broke up as they moved downhill, and intact landslide toes were rare. Most of the landslide toes were jumbled masses of soil and rock that blanketed underlying vegetation with shallow deposits. Unlike purely rotational or translational landslides, the observed slides demonstrate a transition from sliding to flowing because the landslide bodies did not remain intact.

The depth measured at landslide scarps in the field ranged from 0.15 to 0.5 m, with an average depth of 0.35 m. Failure planes appeared to coincide with the contact between soil and underlying saprolite. The saprolite layer is highly weathered and considerably more cohesive than the overlying soil, but rills were carved into the saprolite at some of the landslide scars. The average rooting depth measured at exposed landslide locations was 0.26 m.

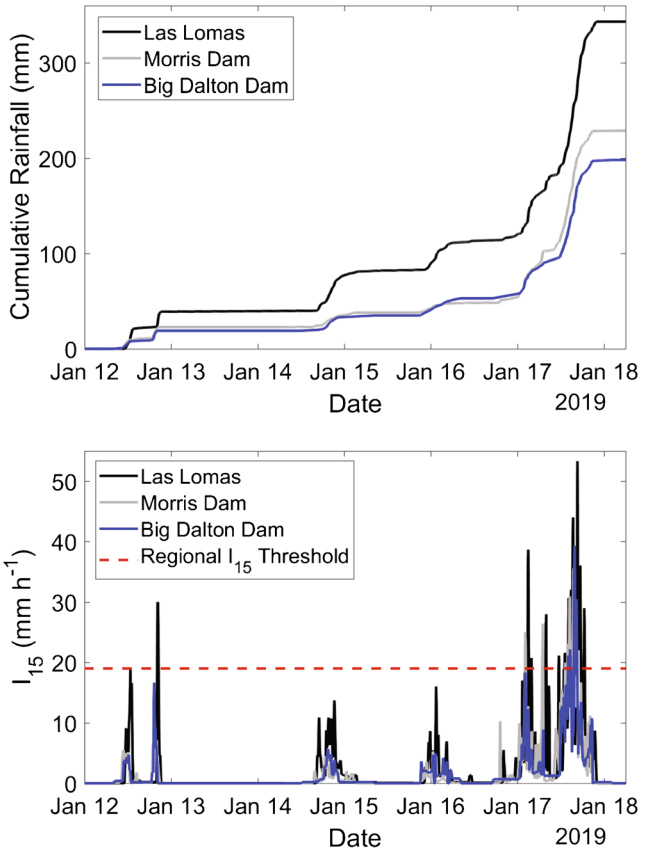

Fig. 2 Cumulative rainfall during the landslide-triggering storm from three rain gages near the study area (top). The Las Lomas and Morris Dam gages are shown in Fig. 1, and the Big Dalton Dam (34.17265, − 117.80834) is located about 5 km east of the Morris Dam gage (outside of the study area). A 15-min rainfall intensity at the three rain gages compared with the year 1 regional 15-min rainfall intensity threshold for runoff-generated debris flows in Southern California (bottom) (Staley et al. 2017)

Mass movement volume year 1 versus year 3

We estimated total volumes from three runoff-generated debris flows in year 1 (Staley et al. 2018) in the Las Lomas basin (Fig. 1). The year 1 runoff-generated debris flows mobilized 3200, 2500, and 2100 m^3 of sediment following rainstorms with peak 15-min intensities of 26.4, 28.8, and 36 mm h^{-1}, respectively. For comparison, the shallow landslides in year 3 mobilized only 160 m^3 in the same Las Lomas basin following a storm with a maximum 15-min rainfall intensity of 53 mm h^{-1} (Fig. 2 and Table 1).

Landslide density

The vast majority of landslides (98%) were observed in the burned areas; only 2% of the mapped landslides were in the unburned parts of the study area despite the fact that the unburned area (38 km^2) represents 54% of the study area. In addition, burn severity strongly influences landslides: 69% of the landslide polygons were completely burned at moderate to high severity over 90% of the landslide polygon area (Fig. 3). Moreover, only 12% of the landslide polygons occupied areas that were a combination of unburned and low severity, without any moderate or high burn severity.

In addition, the landslide scarp density following the storm on 16–17 January 2019 differs distinctly depending on the time since wildfire (Fig. 4). The most recent fire, the 2016 SGC, had a landslide scarp density of 11.8 landslide scarps per square kilometer. In contrast, the area burned in the 2014 Colby fire only had 0.8 landslide scarps per square kilometer, and the unburned areas had 0.2 landslide scarps per square kilometer. The area that burned in the 2009 Morris fire and then reburned in the 2016 SGC fire had 11.6 landslide scarps per square kilometer (Fig. 4).

Landslide aspect and slope

Landslide mapping revealed that most landslides occurred on steep, south-facing slopes. The pre-failure median slope angle at the locations of the landslide main scarps was 39.5° (Fig. 5), which is slightly higher than the average slope angle in each of the individual wildfire area (Table 2). In addition, 95% of the landslides occurred on south-facing (90–270°) slopes (Fig. 5), although south-facing slopes are limited to approximately 60% of each of the burn area (Table 2).

Landslide runout

The tangent of the angle of reach (H/L) for all of the year 3 landslides in this study is 0.89, with maximum and minimum

Table 1 Cumulative rainfall and maximum 15-min rainfall intensity measured at the Las Lomas rain gage from 12 to 17 January 2019

Date	Cumulative rainfall (mm)	Maximum 15-min rainfall intensity (mm/h)
2019-01-12	40.0	28.0
2019-01-13	40.0	0.0
2019-01-14	78.0	16.0
2019-01-15	91.0	16.0
2019-01-16	121.0	40.0
2019-01-17	344.0	53.0

values of 1.5 and 0.26, respectively (Fig. 6a). The Kruskal–Wallis test of four different groups of landslide H/L distributions (fire in 2016, fire in both 2009 and 2016, fire in 2014, and unburned) returned a value of $p = 0.13$. This result demonstrates that landslide mobility was not statistically different at a significance level of $\alpha = 0.1$ between landslides in burned versus unburned areas or in areas that burned at different times.

The mobility of the landslides in year 3 contrasted strongly with the debris flows that were observed in year 1 (Fig. 6). The median H/L of the year 1 debris flows in the Van Tassel watershed (Fig. 1) was 0.14 with maximum and minimum values of 0.2 and 0.06 (Fig. 6b). Here, we used evidence of debris flow deposition at the canyon outlet (Fig. 7) to establish a debris flow deposition point and assumed that the debris flows were initiated at the channel heads.

Discussion

Observations from this study demonstrate that wildfire influences landslide initiation in this study area within a relatively short time window, and the link between wildfire and landsliding declines rapidly with time due to vegetation recovery. Temporal changes in soil infiltration rates may also play a role. At our study site, the first-year response to rainfall resulted in runoff-generated debris flows that mobilized large volumes of sediment and deeply scoured the channels (Staley et al. 2018; Tang et al. 2019). However, infiltration rates generally increase to values near pre-fire conditions after 1–3 years (Mayor et al. 2007; Moody and Martin 2001). Within the Las Lomas watershed at our site, we found that the wetting front suction head, a parameter that controls infiltration rates in the Green–Ampt infiltration model, increased by an order of magnitude over an 18-month period from September 2016 to March 2018 (McGuire et al. 2019). Therefore, wildfire-induced reductions in soil infiltration capacity, which promoted infiltration excess overland flow in year 1, were not as strong by year 3. Therefore, when a long-duration rainstorm with peak 15-min rainfall intensities between 40 and 53 mm/h moved over our study site in the third year following wildfire, we observed landslides in the most recently burned area, rather than runoff-generated debris flows. This contrast is particularly striking since the rainfall intensities that triggered runoff-generated debris flows in the first year after the fire had lower peak 15-min rainfall intensities (26.4–36 mm/h).

This study points toward a lagged peak in the amount of sediment derived from shallow landsliding after fire, similar to the influence of timber harvest on landsliding (Sidle 2005). We propose a possible conceptual model with three distinct time periods (no recovery, initial recovery, and fully recovered). During the no recovery period, the water repellency initially after wildfire delays infiltration-related landsliding. At a slightly longer timescale after the fire during the initial recovery phase, infiltration rates recover allowing more water into the subsurface, creating a higher probability of the positive pore water pressures needed during rainstorms to induce landsliding. Simultaneously, roots decay, which reduces the apparent root cohesion and provides less resistance against landsliding. Finally, in the fully recovered phase, as new vegetation roots are established, hillslopes stabilize again. Rice (1982) uses the same conceptual model of increasing infiltration with time since wildfire to explain observations of

Fig. 3 Histogram showing the percentage of each landslide polygon burned at moderate to high severity

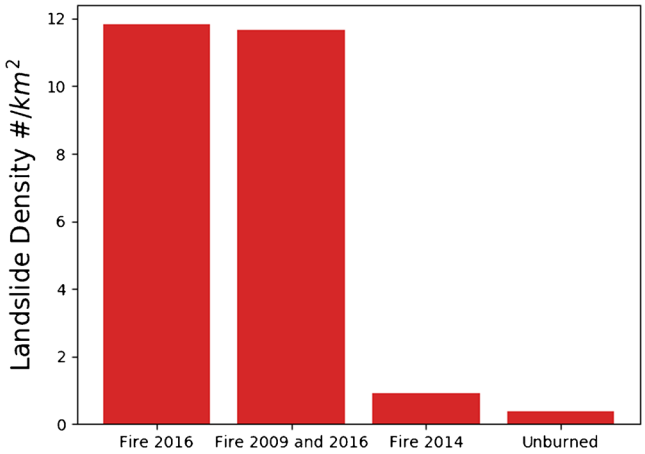

Fig. 4 Density of landslide scarps per square kilometer based on the time since fire. The fires in this histogram are SGC fire (2016), Morris fire (2009), and Colby fire (2014)

differing landslide-driven erosion rates in three watersheds within the San Gabriel Mountains following a rainstorm in 1969. Erosion attributable to landslides was 16 m^3/ha in a watershed that had not burned in the last 50 years (fully recovered), 10 m^3/ha in a watershed that burned the year prior to the storm (no recovery), and 298 m^3/ha in a watershed that burned 9 years before the storm (initial recovery) (Rice 1982). At our study site, the landslide-driven erosion rate from the 16–17 January 2019 rainstorm at the Las Lomas basin was 8 m^3/ha, which is slightly less than what has been observed during other cases of widespread shallow landslide activity in the San Gabriel Mountains (Rice 1982), and much

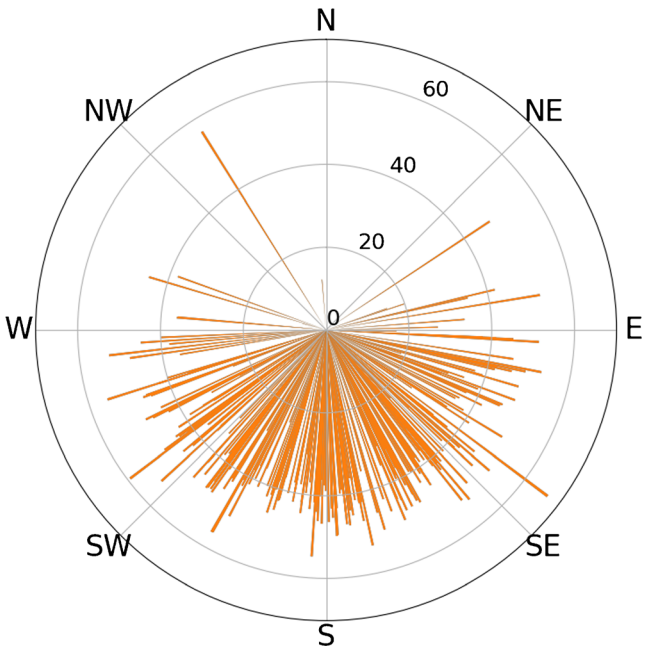

Fig. 5 Polar plot where each line represents a single landslide. The line length indicates the slope angle (degrees) at the location of each landslide scarp prior to failure. The corresponding cardinal direction of the landslide aspect is indicated by the angle that the lines are plotted

Table 2 Slope and aspect characteristics by the fire area

Fire	Mean slope (degrees)	% south-facing
San Gabriel Complex	37.7	61%
Morris	34.1	61%
Colby	35.9	66%

smaller than the volume of the debris flow–transported sediment in year 1 (Staley et al. 2018).

We found that the landslide density varied strongly with number of years of post-fire recovery. The area that burned 5 years prior to the rainstorm had a much lower density of landsliding than the area burned 3 years prior, presumably because of the longer time for root strength recovery from vegetation regrowth (Fig. 4). In fact, the landslide density in the 2014 Colby fire (0.8 landslide per km^2) was much closer to the density in the unburned area (0.2 landslide per km^2) than to that in the 2016 SGC fire (11.8 landslide per km^2). In addition, the part of the Morris fire that burned in the 2009 fire and then reburned in 2016 had a similar landslide density (11.6 landslide per km^2) to the rest of the 2016 burn area that was not a recent reburn. This shows that, in this region, after approximately 5 years, vegetation recovery may be sufficient to reduce landslide risks to levels near those of background rates in unburned terrain. Consequently, the landscape is most susceptible to landsliding during a short temporal window between the time required for hydrologic recovery and vegetation recovery (i.e., 3–5 years at this study site). We refer to this as the initial recovery phase in our conceptual model.

Another major finding from this study was that the overwhelming majority of landslides occurred in areas that were burned at moderate/high severity (Fig. 3). These data show that landslide initiation, even several years following fire, is strongly controlled by burn severity. As the site recovers, we hypothesize that the moderate and high burn severity areas have lower vegetation density, weaker root strength, and less rainfall interception (i.e., rain captured by vegetation leaves and branches) relative to areas burned at low severity. In this case, the rainfall could infiltrate moderate/high-severity burn areas faster than in the immediate post-fire condition, but the recovering vegetation might not have the strength to prevent soil instability during large rainstorms. Consequently, post-wildfire landslide susceptibility appears to be linked to the stage of vegetation recovery.

We also see a strong aspect control on landsliding. The aspect dependence could reflect the storm direction, which impacted the area while moving primarily from south to north. But it also could reflect the vegetation density contrast between the south- and north-facing aspects. For example, different hillslope aspects were burned at moderate severity 3 years prior (Fig. 8a). The post-fire south-facing slopes show lower vegetation density as well as landslides, whereas the north-facing slopes show higher vegetation densities and no landslides. The denser vegetation and associated root strength on north-facing slopes provide an explanation for the relative paucity of landslides on north-facing slopes (5%) compared with south-facing slopes (95%). This aspect dependence contrasts strongly with the first-year, runoff-generated debris flows that did not have any notable aspect dependence.

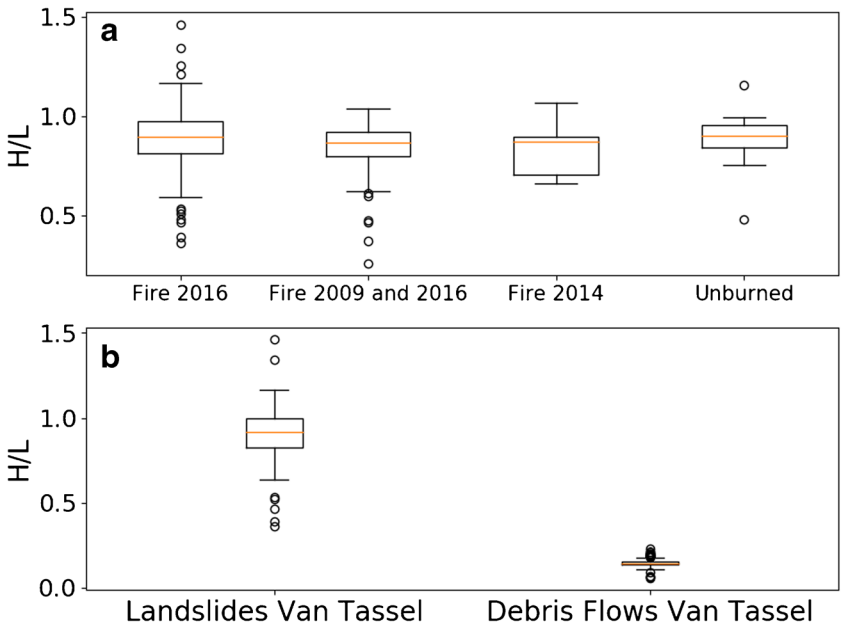

Fig. 6 Box-and-whisker plot for the tangent of the angle of reach (*H*/*L*) of landslides. **a** Landslides grouped by wildfire timing. **b** Landslides and debris flows in the Van Tassel (VT) watershed in year 1 after wildfire

In contrast to the aspect, the geology seems to exert little control on the landslide distribution. Within the SGC fire perimeter, slides occur in both the San Gabriel River tonalite and a layered gneiss unit (Morton and Miller 2003). In the Colby fire, landslides are concentrated in the leucocratic and granitic rocks, and the slides in the Morris fire reburned by the SGC fire are in the Pelona Schist and a gneissic granodiorite (Morton and Miller 2003). This corresponds to the prior observations in the San Gabriel Mountains that rock type may not strongly influence erosion and that erosion rates may be more strongly tied to fracturing due to tectonic deformation (Lifton and Chase 1992; Pelletier 2017; Spotila et al. 2002).

Meteorological characteristics of the storm that initiated the landslides (16–17 January 2019), though favorable for intense precipitation, are less likely to have played a role in the landslide spatial distribution. This storm event was associated with an atmospheric river, which is characterized by moist low-level flow and a moist-neutral stability profile (e.g., Ralph et al. 2005). The event also featured low-level southerly winds roughly orthogonal to the trend of the San Gabriel Mountains. These characteristics, combined with the location of the study area in a region of general concavity in the range (Fig. 1), create conditions favorable for intense orographic rainfall along the windward (southern) slopes of the San Gabriel Mountains (Lin et al. 2001). Additionally, such conditions have been demonstrated as characteristic of storm events producing precipitation that exceeds various published landslide-triggering thresholds in the San Gabriel Mountains (Oakley et al. 2018). However, the orographic precipitation processes described operate on the scale of a few to tens of kilometers, represent enhanced precipitation along the windward side of the mountain range, and are not likely to describe variations in landslide aspect over slope-scale distances (< 1 km) as observed in this study. High-resolution atmospheric simulations would be needed to definitively rule out meteorological characteristics as a driver of landslide distribution and are currently beyond the scope of this study. Moreover, this was not the first atmospheric river to hit the area since the 2016 SGC fire, but it was the only storm that produced shallow landsliding.

In addition to the primary atmospheric river–related precipitation event described above, if we include rainfall from several days prior, the cumulative rainfall amounts are between 200 and 340 mm. Prior observations show that landsliding in Southern California typically requires a threshold of 254 mm of winter season precipitation followed by a burst of 6.4 mm of rainfall in 1 h before the onset of widespread landsliding (Campbell 1975). In this study, the total rainfall measured at the Las Lomas gage between 1 October 2018 and the end of the rainstorm on 18 January 2019 was more than 600 mm, and there was a burst of 34 mm of rainfall in 1 h, well above the threshold proposed in Campbell (1975).

Despite the ubiquity of new landslides, most of the slides are relatively small and have a short runout distance. The *H*/*L* values in the burned versus unburned landslides, which represent the mobility of mass failure, appeared similar. Moreover, the low mobility of the landslides is likely related to the small volume of material that was mobilized (Iverson 1997; Legros 2002). The angle of reach can be considered a proxy for the angle of friction (Scheidegger 1973). In this study, the median angle of friction for the slides would be 41.7 degrees, which corresponds closely to the median slope angle at the location of the landslide main scarps prior to failure (39.5 degrees) and indicates slope parallel failure. Both the magnitude of the mobilized volumes in the year 3 landslides and the mobility of the mass movements were orders of magnitude smaller than the volumes observed in the year 1 runoff-generated debris flows. Because the landslides initiated on hillslopes close to the top of the ridges and most of the concentrated debris flow erosion occurred in channels farther

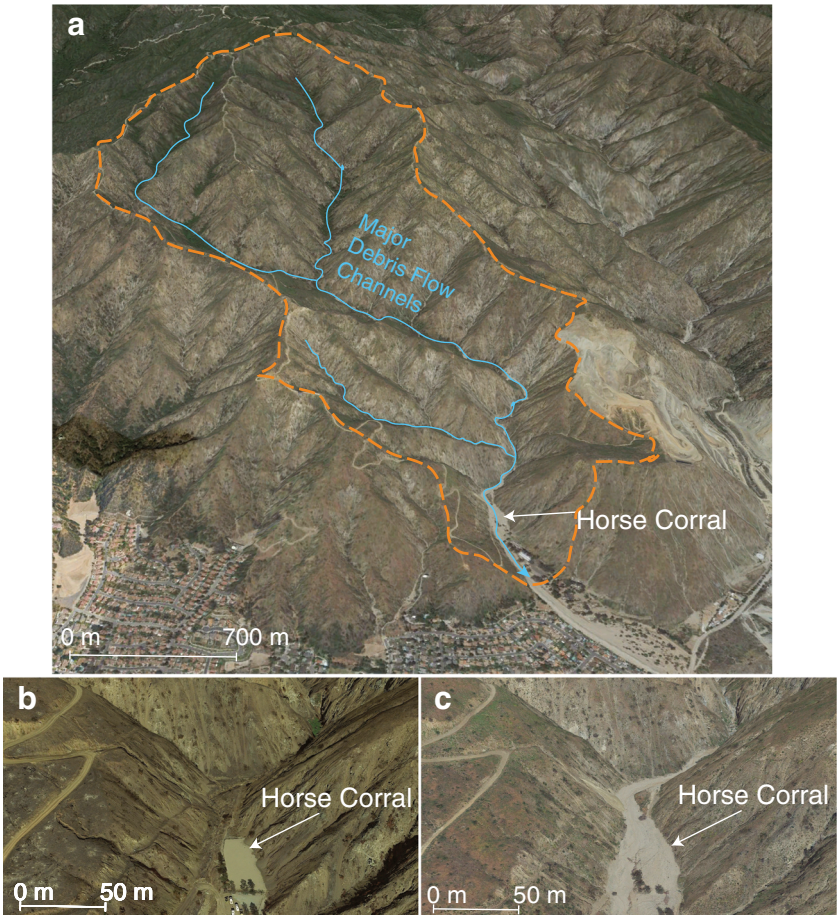

Fig. 7 **a** Google Earth imagery showing an overview of the Van Tassel watershed on 28 April 2017 in year 1 after the fire and after the first rainy season following the wildfire. Dashed line shows the watershed boundaries, and blue lines indicate the primary pathways for debris flow sediment. **b** Google Earth imagery showing a closeup view of the canyon outlet of the Van Tassel watershed on 18 October 2016, after the SGC fire and before any significant rainfall. **c** Google Earth imagery showing a closeup view of the canyon outlet of the Van Tassel watershed on 28 April 2017, after the fire and after the first rainy season following the wildfire. Note the debris flow sediment deposition in the horse corral

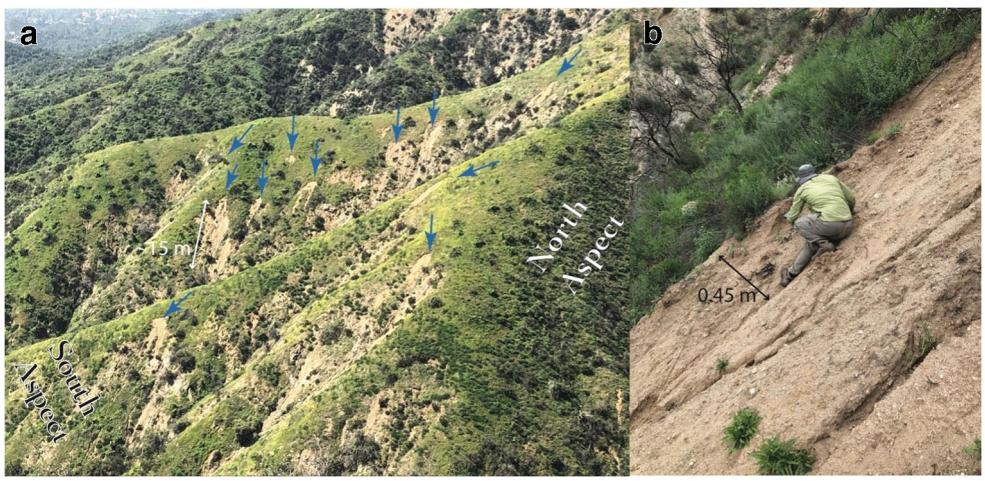

Fig. 8 **a** Photo showing shallow landslides in the study area. Blue arrows indicate landslide scarps. **b** View near the scarp of one landslide with the depth of the landslide release zone indicated (photo credit. F. Rengers)

downstream, the areas affected by these two mass movement processes have little spatial overlap. Moreover, because debris flows are more fluid and travel through a confined drainage, one would expect the tangent of the angle of reach to be lower than those observed from landsliding. Because of the differences between landslide and debris flow processes, it is of limited value to directly compare the angle of reach for the two types of mass movements. Nevertheless, the observed values of *H*/*L* in this study may lead to helpful insights in estimating the angle of reach for future post-fire landslides and debris flows, respectively. The post-fire shallow landsliding from the 16–17 January 2019 storm was not particularly hazardous to life or infrastructure in our study area, but it played an important geomorphic role in reloading downstream channels with sediment, priming the system for future debris flows, and providing the tools necessary for bedrock channel erosion.

Conclusion

In this study, we mapped 286 landslides on steep slopes composed of both burned and unburned areas. The burned areas included regions that burned 3 years prior to the landslide-producing storm, 5 years prior, and slopes that had burned twice in the recent past (10 years prior to the storm and again 3 years prior). The landslide density was the highest in areas that burned 3 years prior to the storm. Reburned areas had a similar landslide density, revealing that reburning did not create a higher susceptibility to landsliding. In addition, the area burned 5 years prior to the storm had a landslide density closer to the unburned area, which shows that wildfire-enhanced susceptibility to landsliding was gone after 5 years. Moreover, landslide scarps were mostly located on steep, south-facing slopes, which may indicate that the vegetation recovery on north-facing slopes was sufficient to prevent landsliding. Consequently, there appears to be a brief temporal window when the landscape is particularly vulnerable to landslides between the time it takes for partial hydrologic recovery and the time it takes for vegetation recovery. The initial landscape response after the fire was in the form of runoff-generated debris flows. Partial hydrologic recovery is required so that post-wildfire rainfall is primarily infiltrating into the soil rather than running off (a key requirement to generate landslides), and vegetation recovery allows roots to increase the apparent cohesion of the soil, reducing the likelihood of landslides. Despite the ubiquity of landslides in the study area, the total landslide travel distances were short, and the volumes and mobility of the shallow landslides were much smaller than those associated with the runoff-generated debris flows in the first year after wildfire.

Acknowledgments

We would like to gratefully acknowledge Kelsha Anderson (U.S. Forest Service) for her help providing access to the Angeles National Forest.

Funding information McGuire and Oakley were supported in part by the National Oceanic and Atmospheric Administration (NOAA) National Integrated Drought Information System (NIDIS) through Task Order 1332KP20FNRMT0012.Data availabilityData for this study are available through the USGS ScienceBase (Rengers 2020).

Compliance with ethical standards

Disclosure Any use of trade, firm, or product names is for descriptive purposes only and does not imply endorsement by the US Government.

References

Attal M, Mudd SM, Hurst MD, Weinman B, Yoo K, Naylor M (2015) Impact of change in erosion rate and landscape steepness on hillslope and fluvial sediments grain size in the Feather River basin (Sierra Nevada, California). Earth Surf Dyn 3:201–222

Benda L, Dunne T (1997) Stochastic forcing of sediment supply to channel networks from landsliding and debris flow. Water Resour Res 33:2849–2863

Campbell RH (1975) Soil slips, debris flows, and rainstorms in the Santa Monica Mountains and vicinity, Southern California. U.S. Geological Survey Professional Paper 851, 51 p. https://doi.org/10.3133/pp851

Cannon S, Gartner JE, Rupert MG, Michael JA, Rea AH, Parrett C (2010) Predicting the probability and volume of postwildfire debris flows in the intermountain Western United States. Geol Soc Am Bull 122:127–144

Cocke AE, Fulé PZ, Crouse JE (2005) Comparison of burn severity assessments using differenced normalized burn ratio and ground data. Int J Wildland Fire 14:189–198

Coe JA, Bessette-Kirton EK, Geertsema M (2018) Increasing rock-avalanche size and mobility in Glacier Bay National Park and Preserve, Alaska detected from 1984 to 2016 Landsat imagery. Landslides 15:393–407

Corbett ES, Rice RM (1966) Soil slippage increased by brush conversion. Res. Note PSW-RN-128, vol 8. U.S. Department of Agriculture, Forest Service, Pacific Southwest Forest and Range Experiment Station, Berkeley, p 128

Corominas J (1996) The angle of reach as a mobility index for small and large landslides. Can Geotech J 33:260–271

Dai FC, Lee CF (2002) Landslide characteristics and slope instability modeling using GIS, Lantau Island, Hong Kong. Geomorphology 42:213–228

De Graff JV (2018) A rationale for effective post-fire debris flow mitigation within forested terrain. Geoenviron Disasters 5:1–9

DeBano LF (2000) The role of fire and soil heating on water repellency in wildland environments: a review. J Hydrol 231:195–206

DeBano LF, Rice RM, Eugene CC et al (1979) Soil heating in chaparral fires: effects on soil properties, plant nutrients, erosion, and runoff (No. Berkeley, CA). U.S. Forest Service Research Paper (RP-145)

Densmore AL, Anderson RS, McAdoo BG, Ellis MA (1997) Hillslope evolution by bedrock landslides. Science 275:369–372

Dowling CA, Santi PM (2014) Debris flows and their toll on human life: a global analysis of debris-flow fatalities from 1950 to 2011. Nat Hazards 71:203–227

Eaton EC (1935) Flood and erosion control problems and their solution. Trans Am Soc Civ Eng 101:1302–1330

Ebel BA, Moody JA (2016) Synthesis of soil-hydraulic properties and infiltration time-scales in wildfire-affected soils. Hydrol Process 31:324–340

Egholm DL, Knudsen MF, Sandiford M (2013) Lifespan of mountain ranges scaled by feedbacks between landsliding and erosion by rivers. Nature 498:475–478

Froude MJ, Petley D (2018) Global fatal landslide occurrence from 2004 to 2016. Nat Hazards Earth Syst Sci 18:2161–2181

Gehring E, Conedera M, Maringer J, Giadrossich F, Guastini E, Schwarz M (2019) Shallow landslide disposition in burnt European beech (Fagus sylvatica L.) forests. Sci Rep 9, page range

Gillett NP, Weaver AJ, Zwiers FW, Flannigan MD (2004) Detecting the effect of climate change on Canadian forest fires. Geophys Res Lett 31, page range

Halsey RW (2005) Fire, chaparral, and survival in Southern California. Sunbelt Publications

Helvey JD (1980) Effects of a North Central Washington wildfire on runoff and sediment production 1. J Am Water Resour Assoc 16:627–634
Hu FS, Higuera PE, Walsh JE, Chapman WL, Duffy PA, Brubaker LB, Chipman ML (2010) Tundra burning in Alaska: linkages to climatic change and sea ice retreat. J Geophys Res: Biogeosci 115, page range
Hudak AT, Robichaud P, Evans JS, Clark J, Lannom K, Morgan P, Stone C (2004) Field validation of burned area reflectance classification (BARC) products for post fire assessment, more details needed
Hyde KD, Wilcox AC, Jencso K, Woods S (2014) Effects of vegetation disturbance by fire on channel initiation thresholds. Geomorphology 214:84–96
Iverson RM (1997) The physics of debris flows. Rev Geophys 35:245–296
Jackson M, Roering JJ (2009) Post-fire geomorphic response in steep, forested landscapes: Oregon Coast Range, USA. Quat Sci Rev 28:1131–1146. https://doi.org/10.1016/j.quascirev.2008.05.003
Kasischke ES, Turetsky MR (2006) Recent changes in the fire regime across the North American boreal region—spatial and temporal patterns of burning across Canada and Alaska. Geophys Res Lett 33 page range
Kean JW, Staley DM, Lancaster JT, Rengers FK, Swanson BJ, Coe JA, Hernandez JL, Sigman AJ, Allstadt KE, Lindsay DN (2019a) Inundation, flow dynamics, and damage in the 9 January 2018 Montecito debris-flow event, California, USA: opportunities and challenges for post-wildfire risk assessment. Geosphere 15:1140–1163. https://doi.org/10.1130/GES02048.1
Kean JW, Smith JB, Rengers FK, McGuire LA, Staley DM (2019b) Post-wildfire debris-flow monitoring data, Las Lomas, 2016 Fish Fire, Los Angeles County, California, November 2016 to February 2017. U.S. Geological Survey data release. https://doi.org/10.5066/P9F3YTBP.
Key CH, Benson NC (2004) Landscape assessment: remote sensing of severity, the normalized burn ratio and ground measure of severity, the composite burn index. In: Lutes DC, Keane RE, Caratti JF, Key CH, Benson NC, Gangi LJ (eds) FIREMON: fire effects monitoring and inventory system, General Technical Report RMRS-GTR-164-CD; LA-1-55. U.S. Department of Agriculture, Forest Service, Rocky Mountain Research Station, Ogden
Korup O (2004) Landslide-induced river channel avulsions in mountain catchments of southwest New Zealand. Geomorphology 63:57–80
Kotok EI, Kraebel CJ (1935) Discussion of "Flood and erosion control problems and their solution." American Society of Civil Engineers Transactions 101:1350–1355
Kummerow J, Krause D, Jow W (1977) Root systems of chaparral shrubs. Oecologia 29:163–177
Lanini JS, Clark EA, Lettenmaier DP (2009) Effects of fire-precipitation timing and regime on post-fire sediment delivery in Pacific Northwest forests. Geophys Res Lett 36 page range
Lavé J, Burbank D (2004) Denudation processes and rates in the Transverse Ranges, Southern California: erosional response of a transitional landscape to external and anthropogenic forcing. J Geophys Res: Earth Surf 109 page range.
Legros F (2002) The mobility of long-runout landslides. Eng Geol 63:301–331
Lévy S, Jaboyedoff M, Locat J, Demers D (2012) Erosion and channel change as factors of landslides and valley formation in Champlain Sea clays: the Chacoura River, Quebec, Canada. Geomorphology 145:12–18
Lifton NA, Chase CG (1992) Tectonic, climatic and lithologic influences on landscape fractal dimension and hypsometry: implications for landscape evolution in the San Gabriel Mountains, California. Geomorphology 5:77–114
Lin Y-L, Chiao S, Wang T-A, Kaplan ML, Weglarz RP (2001) Some common ingredients for heavy orographic rainfall. Weather Forecast 16:633–660
Martin YE (2007) Wildfire disturbance and shallow landsliding in coastal British Columbia over millennial time scales: a numerical modelling study. Catena 69:206–219
May CL, Gresswell RE (2003) Processes and rates of sediment and wood accumulation in headwater streams of the Oregon Coast Range, USA. Earth Surf Process Landf 28:409–424
Mayor AG, Bautista S, Llovet J, Bellot J (2007) Post-fire hydrological and erosional responses of a Mediterranean landscpe: seven years of catchment-scale dynamics. Catena 71:68–75
McGuire LA, Rengers FK, Kean JW, Staley DM, Mirus BB (2018) Incorporating spatially heterogeneous infiltration capacity into hydrologic models with applications for simulating post-wildfire debris flow initiation. Hydrol Process 32:1173–1187
McGuire LA, Rengers FK, Kean JW, Staley DM, Tang H, Youberg AM (2019) Looking through the window of disturbance at post-wildfire debris flow hazards, in: Association of Environmental and Engineering Geologists; Special Publication 28. Colorado School of Mines. Arthur Lakes Library
Meyer GA, Pierce JL, Wood SH, Jull AT (2001) Fire, storms, and erosional events in the Idaho Batholith. Hydrol Process 15:3025–3038
Miller JD, Safford HD, Crimmins M, Thode AE (2009) Quantitative evidence for increasing forest fire severity in the Sierra Nevada and southern Cascade Mountains, California and Nevada, USA. Ecosystems 12:16–32
Moody JA, Martin DA (2001) Initial hydrologic and geomorphic response following a wildfire in the Colorado Front Range. Earth Surf Process Landf 26:1049–1070
Morton DM, Miller FK (2003) Preliminary geologic map of the San Bernardino 30′ x 60′ quadrangle, California. U.S. Geological Survey Open-File Report 03-293
Nyman P, Sheridan GJ, Moody JA, Smith HG, Noske PJ, Lane PN (2013) Sediment availability on burned hillslopes. J Geophys Res Earth Surf 118:2451–2467
Oakley NS, Lancaster JT, Hatchett BJ, Stock J, Ralph FM, Roj S, Lukashov S (2018) A 22-year climatology of cool season hourly precipitation thresholds conducive to shallow landslides in California. Earth Interact 22:1–35
Ouimet WB, Whipple KX, Royden LH, Sun Z, Chen Z (2007) The influence of large landslides on river incision in a transient landscape: eastern margin of the Tibetan Plateau (Sichuan, China). Geol Soc Am Bull 119:1462–1476
Parsons A, Robichaud PR, Lewis SA, Napper C, Clark JT (2010) Field guide for mapping post-fire soil burn severity. Gen. Tech. Rep. RMRS-GTR-243. Fort Collins, CO: U.S. Department of Agriculture, Forest Service, Rocky Mountain Research Station. 49 p 243
Pausas JG, Fernández-Muñoz S (2012) Fire regime changes in the Western Mediterranean Basin: from fuel-limited to drought-driven fire regime. Clim Chang 110:215–226
Pelletier JD (2017) Quantifying the controls on potential soil production rates: a case study of the San Gabriel Mountains, California, more details needed
Petley D (2012) Global patterns of loss of life from landslides. Geology 40:927–930
Ralph FM, Neiman PJ, Rotunno R (2005) Dropsonde observations in low-level jets over the northeastern Pacific Ocean from CALJET-1998 and PACJET-2001: mean vertical-profile and atmospheric-river characteristics. Mon Weather Rev 133:889–910
Regelbrugge JC, Conard SG (1993) Modeling tree mortality following wildfire in Pinus ponderosa forests in the central Sierra-Nevada of California. Int J Wildland Fire 3:139–148
Rengers FK (2020) Inventory of landslides triggered by rainfall on 16-17 January 2019, Los Angeles County, CA. https://doi.org/10.5066/P97GU3UV
Rengers FK, Pagonis V, Mahan SA (2017) Can thermoluminescence be used to determine soil heating from a wildfire? Radiat Meas 107:119–127
Rice RM (1982) Sedimentation in the chaparral: how do you handle the unusual events? In: Swanson FJ, Janda RJ, Dunne T, Swanston DN (eds) Sediment Budgets and Routing in Natural System, General Technical Report PNW-141. United States Department of Agriculture, Pacific Northwest Forest and Range Experiment Station, pp 39–49
Rice RM, Foggin GT III (1971) Effect high intensity storms on soil slippage on mountainous watersheds in Southern California. Water Resour Res 7:1485–1496
Rickenmann D (2005) Runout prediction methods. In: Debris-Flow Hazards and Related Phenomena. Springer, pp 305–324
Scheidegger AE (1973) On the prediction of the reach and velocity of catastrophic landslides. Rock Mech Rock Eng 5:231–236
Schmidt KM, Montgomery DR (1995) Limits to relief. Science 270:617–620
Scott KM (1971) Origin and sedimentology of 1969 debris flows near Glendora, California. U.S. Geol Surv Prof Pap 750:242–247
Sidle RC (2005) Influence of forest harvesting activities on debris avalanches and flows. In: Debris-Flow Hazards and Related Phenomena. Springer, pp 387–409
Spotila JA, House MA, Blythe AE, Niemi NA, Bank GC, Barth A (2002) Controls on the erosion and geomorphic evolution of the San Bernardino and San Gabriel Mountains, Southern California. Special Papers-Geological Society of America 205–230. https://doi.org/10.1130/0-8137-2365-5.205

Staley DM, Kean JW, Cannon SH, Schmidt KM, Laber JL (2013) Objective definition of rainfall intensity–duration thresholds for the initiation of post-fire debris flows in Southern California. Landslides 10:547–562
Staley DM, Negri JA, Kean JW, Laber JL, Tillery AC, Youberg AM (2017) Prediction of spatially explicit rainfall intensity–duration thresholds for post-fire debris-flow generation in the Western United States. Geomorphology 278:149–162
Staley DM, Tillery AC, Kean JW, McGuire LA, Pauling HE, Rengers FK, Smith JB (2018) Estimating post-fire debris-flow hazards prior to wildfire using a statistical analysis of historical distributions of fire severity from remote sensing data. Int J Wildland Fire 27:595–608
Tang H, McGuire LA, Rengers FK, Kean JW, Staley DM, Smith JB (2019) Evolution of debris flow initiation mechanisms and sediment sources during a sequence of post-wildfire rainstorms. J Geophys Res 124:1572–1595. https://doi.org/10.1029/2018JF004837
Varnes DJ (1978) Slope movement types and processes. In: Schuster RL, Krizek RJ (eds) Landslides—analysis and control: National Research Council, Washington, D.C., Transportation Research Board, Special Report 176, p 11–33
Web Soil Survey [WWW Document] (2020) URL https://websoilsurvey.sc.egov.usda.gov/App/WebSoilSurvey.aspx. Accessed 5.11.20
Wells WG (1987) The effects of fire on the generation of debris flows in Southern California. Rev Eng Geol 7:105–114
Westerling AL, Hidalgo HG, Cayan DR, Swetnam TW (2006) Warming and earlier spring increase western U.S. forest wildfire activity. Science 313:940–943
Woodsmith RD, Vache KB, McDonnell JJ, Helvey JD (2004) Entiat Experimental Forest: catchment-scale runoff data before and after a 1970 wildfire. Water Resour Res 40, page range
Woodsmith RD, Vache KB, McDonnell JJ, Seibert J, Helvey JD (2007) The Entiat Experimental Forest: a unique opportunity to examine hydrologic response to wildfire. In: Furniss MJ, Clifton C, Ronnenberg KL (eds) Advancing the Fundamental Sciences: Proceedings of the Forest Service National Earth Sciences Conference. Portland: U.S. Department of Agricultire, Forest Service, Pacific Northwest Research Station: no. 205-216. pp 205–216

F. K. Rengers (✉) · **J. W. Kean** · **D. M. Staley**
Landslide Hazards Program, Geologic Hazards Science Center,
U.S. Geological Survey,
Golden, CO 80401, USA
Email: frengers@usgs.gov

L. A. McGuire
Department of Geosciences,
University of Arizona,
Tucson, AZ 85721, USA

N. S. Oakley
Center for Western Weather and Water Extremes, Scripps Institution of Oceanography,
University of California, San Diego,
San Diego, CA 92037, USA

H. Tang
German Research Centre for Geosciences, Helmholtz Center,
14473, Potsdam, Germany